Chinese Chemical Letters 32 (2021) 1456–1461

Contents lists available at ScienceDirect

Chinese Chemical Letters

journal homepage: www.elsevier.com/locate/cclet

Communication

# A confined micro-reactor with a movable $Fe_3O_4$ core and a mesoporous $TiO_2$ shell for a photocatalytic Fenton-like degradation of bisphenol A

Pengpeng Qiu[a], Tao Zhao[a], Xiaohang Zhu[a], Binota Thokchom[b], Jianping Yang[a], Wan Jiang[a], Lianjun Wang[a], Yuchi Fan[a], Xiaopeng Li[a,*], Wei Luo[a,*]

[a] State Key Laboratory for Modification of Chemical Fibers and Polymer Materials, College of Materials Science and Engineering, Institute of Functional Materials, Shanghai 201620, China
[b] Indian Institute of Technology Guwahati, Guwahati 781039, India

ARTICLE INFO

*Article history:*
Received 24 August 2020
Received in revised form 21 September 2020
Accepted 30 September 2020
Available online 1 October 2020

*Keywords:*
Photocatalytic Fenton-like reaction
Yolk-shell
Micro-reactor
Magnetic
Mesoporous

ABSTRACT

Photocatalysis and Fenton process are two primary and promising advanced oxidation processes to degrade organic pollutants. However, the practical applications of single photocatalysis and Fenton process are still limited. Introducing one of them into another to form a combined photocatalytic Fenton-like system has shown great potential but still faces challenges in designing a well-tailored catalyst. Herein, a confined photocatalytic Fenton-like micro-reactor catalyst with a movable $Fe_3O_4$ core and a mesoporous $TiO_2$ shell has been constructed *via* a successive Stöber coating strategy, followed by an ultrasound assisted etching method. The resulting micro-reactor possesses well-defined yolk-shell structures with uniform mesopores (~4 nm), a large Brunauer-Emmett-Teller (BET) surface area (~166.7 $m^2/g$), a high pore volume (~0.56 $cm^3/g$) and a strong magnetization (~51 emu/g), as well as tunable reactor sizes (20–90 nm). When evaluated for degrading bisphenol A under solar light in the presence of peroxymonosulfate, the micro-reactor exhibits a superior catalytic degradation performance with a high magnetic separation efficiency and an excellent recycle ability. The outstanding performance can be attributed to its unique textual structure, which leads to a great synergistic effect from the photocatalytic and Fenton-like process. This study gives an important insight into the design and synthesis of an advanced micro-reactor for a combined advanced oxidation processes (AOPs).


Emerging organic contaminants (EOCs) are a kind of contaminants that are not regularly detected but they have high tendency to spread into the environment, which exhibit great potential to cause adverse effects to the ecology and human health. The EOCs are mainly divided into endocrine disruptors, pharmaceuticals and personal care products, surfactants, and various industrial additives as well as hormones [1–3]. Bisphenol A (BPA), classified as an endocrine disruptor, is a tricky pollutant since it has been widely applied in the production of polycarbonates, epoxy resins, and other plastics over the past decade. More importantly, some traditional treatment technologies including adsorption, membrane filtration, and biological treatment are usually restricted to treat them owing to the ultralow concentration, high chemical stability and low biodegradability of BPA [4,5]. As an alternative, advanced oxidation processes (AOPs) have attracted tremendous research interest for the decomposition and mineralization of them through some strong oxidative species such as $^{\bullet}OH$, $^{\bullet}O_2$ [6–9].

Among various AOPs, Fenton-like process based on $Fe^{2+}$ and peroxymonosulfate (PMS) has recently triggered tremendous research interest because of its environmental benignity and cost effectiveness [10–12]. However, the practical application of it is still limited by several drawbacks, such as the narrow operating pH range, hard to recycle the soluble metal ions and necessity for further treatment of sludge [13,14]. To address these problems, the fabrication of a magnetic catalyst is desirable. Up to now, magnetite nanoparticles (NPs) have been widely investigated as one of the most efficient heterogeneous Fenton catalysts among Fe-based nanomaterials due to their higher content of structural $Fe^{2+}$ [15–17]. However, compared with the homogenous Fenton reaction, the catalytic performance of $Fe_3O_4$ NPs based one is still far from expected. Recently, the hybridization of Fenton reaction with photocatalytic process has shown great potential in this field [18–20]. However, the development of a catalyst that could achieve both high Fenton-like and photocatalytic performance is still challenging.

* Corresponding authors.
*E-mail addresses:* xiaopeng.li@dhu.edu.cn (X. Li), wluo@dhu.edu.cn (W. Luo).

https://doi.org/10.1016/j.cclet.2020.09.061

Herein, a unique yolk-shell structured magnetic mesoporous $TiO_2$ has been synthesized through a facile ultrasound assisted etching method and demonstrated as a highly efficient solar photocatalytic Fenton-like catalyst for degrading BPA. The resultant material exhibits a unique yolk-shell structure with uniform mesopores (~4 nm), a large Brunauer-Emmet-Teller (BET) surface area (~166.7 $m^2/g$), a high pore volume (~0.56 $cm^3/g$) and a strong magnetic susceptibility (~51 emu/g). More importantly, the void space can be facilely tuned from 20 nm to 90 nm by changing the thickness (10–46 nm) of $SiO_2$ middle layer, which can act as a superior micro-reactor for the confined photocatalytic Fenton-like degradation of BPA.

The schematic illustration for the synthesis of yolk-shell structured magnetic mesoporous $TiO_2$ micro-reactor are illustrated in Scheme 1. The uniform magnetite NPs are first fabricated *via* a facile solvothermal method, which involves the reduction of Fe(III) salts with ethylene glycol at a high temperature (200 °C) in the presence of sodium citrate as a capping agent. Scanning electron microscope (SEM) images clearly show that the $Fe_3O_4$ NPs exhibit uniform spherical shapes with an average size of ~130 nm (Figs. S1A and B in Supporting information). Owing to the presence of abundant citrate groups on the surface, the NPs possess outstanding dispersibility in water or ethanol, which is very favorable for the subsequent high-quality coating with $SiO_2$ and $TiO_2$. After the first Stöber coating, the $Fe_3O_4$@$SiO_2$ nanospheres with a smooth surface and a particle size of ~200 nm can be obtained (Figs. S1C and D in Supporting information). Transmission electron microscopy (TEM) images reveal that a ~35 nm thick $SiO_2$ layer is evenly wrapped on the $Fe_3O_4$ core, forming a well-defined core-shell structure. The further Stöber coating gives rise to a sandwich-like $Fe_3O_4$@$SiO_2$@$TiO_2$ nanostructure with a uniform $TiO_2$ layer (~35 nm) coated on the $Fe_3O_4$@$SiO_2$ cores (Figs. S1E and F in Supporting information). Following an ultrasound (US) assisted etching process in a weakly basic condition, the $SiO_2$ middle layer in the $Fe_3O_4$@$SiO_2$@$TiO_2$ nanospheres can be completely removed, thus forming the void space between $Fe_3O_4$ core and $TiO_2$ shell. Note that the US can also cause the further hydrolysis of Ti-OR moiety in the $TiO_2$ shell to become complete hydrolyzed form of Ti-OH, leading to the formation of mesoporous structure. The TEM images clearly show that the well-defined yolk-shell nanostructures with a movable black core is obtained (Figs. 1A and B) The overall spacing is measured to be ~70 nm, that equals the thickness of double silica interlayers, indicating that the silica was completely removed in $NaHCO_3$ solution under US irradiation. No Si peak was detected in the X-ray photoelectron spectroscopy (XPS) analysis, further suggesting the complete removal of $SiO_2$ (Fig. S2 in Supporting information). After calcination at 550 °C for 2 h, mesoporous $TiO_2$ micro-reactor with uniform yolk-shell structure was obtained with a highly crystalline

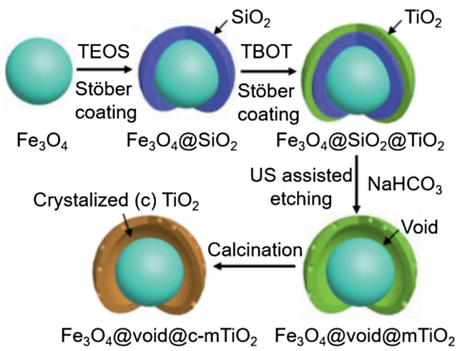


**Scheme 1.** Schematic illustration for the synthesis of magnetic mesoporous $TiO_2$ micro-reactor.

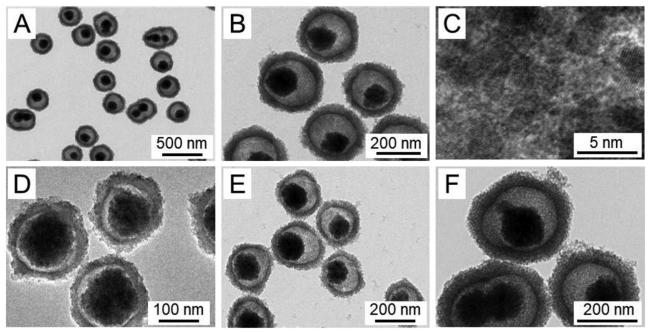


**Fig. 1.** TEM (A and B) HRTEM (C) images of $Fe_3O_4$@$SiO_2$@c-m$TiO_2$-3 and TEM images of $Fe_3O_4$@$SiO_2$@c-m$TiO_2$-1 (D), $Fe_3O_4$@$SiO_2$@c-m$TiO_2$-2 (E) and $Fe_3O_4$@$SiO_2$@c-m$TiO_2$-4 (F).

$TiO_2$ shell. High resolution TEM (HRTEM) image of the $Fe_3O_4$@$SiO_2$@c-m$TiO_2$-3 clearly shows that the $TiO_2$ shell is well crystalized with a d-spacing of 0.35 nm, which is a typical reflection of anatase $TiO_2$ (Fig. 1C). Moreover, the size of the void space can be facilely tuned from 20 nm to 90 nm by adjusting the thickness of $SiO_2$ interlayer from 10 nm to 45 nm (Figs. 1D–F). In previous studies [11], the collapse could occur if the etching of $SiO_2$ did prior to the calcination. However, in our study, the collapse was not observed possibly because the post-hydrolysis of $TiO_2$ shell lead to the formation of void space in the network, which could buffer the thermal expansion during calcination, thus increasing the thermal stability of $TiO_2$ shell. The yolk-shell structured sample with different void space size of 20, 40, 70, 90 nm are denoted as $Fe_3O_4$@void@c-m$TiO_2$-1, $Fe_3O_4$@void@c-m$TiO_2$-2, $Fe_3O_4$@void@c-m$TiO_2$-3, $Fe_3O_4$@void@c-m$TiO_2$-4, respectively.

$N_2$ adsorption-desorption isotherms of the yolk-shell $Fe_3O_4$@void@c-m$TiO_2$-3 NPs (Fig. 2A) depict an IV curve with a hysteresis loops close to H1-type, indicating that the $TiO_2$ shells contain uniform mesopores. The BET surface area and pore volume of the $Fe_3O_4$@void@c-m$TiO_2$-3 sample are measured to be ~166.7 $m^2/g$ and ~0.56 $cm^3/g$, respectively. Correspondingly, the pore size distribution (Fig. 2B) calculated from the adsorption branch using the Barrett-Joyner-Halenda (BJH) method reveals a uniform pore size centered at ~4.2 nm.

X-ray diffraction (XRD) pattern of the $Fe_3O_4$ nanoparticles (Fig. 2C) exhibits several well resolved characteristic diffraction

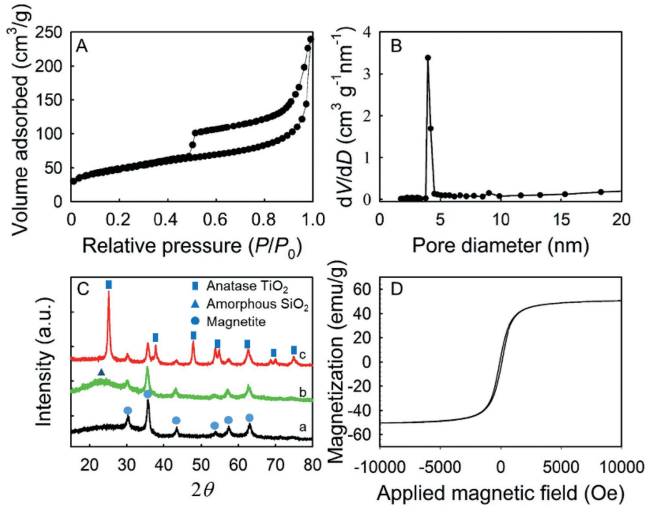


**Fig. 2.** $N_2$ sorption isothermals (A) and pore size distribution (B) of yolk-shell structured mesoporous $TiO_2$ with a void space of 35 nm. XRD patterns (C) of $Fe_3O_4$ (a), $Fe_3O_4$@$SiO_2$ (b), and $Fe_3O_4$@void@m$TiO_2$-3 (c). The magnetic hysteresis loops at 300 K of $Fe_3O_4$@void@m$TiO_2$-3 (D).

peaks, typical for $Fe_3O_4$ crystalline phase. A broad amorphous silica peak can be clearly observed in the XRD pattern of $Fe_3O_4$@$SiO_2$ compared with that of pure $Fe_3O_4$ NPs, suggesting that the $SiO_2$ was coated. No amorphous $SiO_2$ peak was observed in the sample of $Fe_3O_4$@void@m$TiO_2$-3, suggesting that the $SiO_2$ middle layer was well removed. In addition, several sharp peak attributed to anatase $TiO_2$ was detected, proving that the mesoporous $TiO_2$ shell was well crystalized. The magnetic property of the $Fe_3O_4$@void@c-m$TiO_2$-3 micro-reactor was evaluated by measuring the magnetization saturation value (Fig. 2D). As a result of the high magnetization (~51 emu/g), the $Fe_3O_4$@void@c-m$TiO_2$-3 nanospheres in their homogeneous dispersion can be quickly recycled by applying a hand-held magnetic bar (< 30 s, Fig. S3 in Supporting information).

The photocatalytic Fenton-like degradation performance of BPA in the presence of the resultant magnetic mesoporous $TiO_2$ was tested at a neutral pH (Fig. 3A). Before the irradiation of solar light, the system was mechanically stirred in dark for 1 h to achieve an adsorption-desorption equilibrium between the catalyst and BPA. As a control, the degradation performances of BPA under PMS, solar/PMS, solar/catalyst, and PMS/catalyst conditions were also examined, showing the removal efficiencies of 17.0%, 44.5%, 76.1%, 87.1%, respectively. The larger degradation efficiency of solar/PMS process than PMS alone was due to the dissociation of PMS into sulfate radicals through light [21]. When $Fe_3O_4$@void@c-m$TiO_2$-3 micro-reactor were directly used as a Fenton-like catalyst without solar light, the efficiency was significantly improved resulted from the activation of PMS by the surface $Fe^{2+}$. Interestingly, when combine solar light, PMS and $Fe_3O_4$@void@c-m$TiO_2$ catalyst together, the degradation performance of BPA can be greatly promoted, which can achieve a complete degradation within 40 min, demonstrating the priority of this combined process. To better illustrate the priority of the combined process, a synergetic factor ($S$) has been introduced, which can be calculated based on Eq. 1 [22–24].

$$S = \frac{k_{12}}{k_1 + k_2} \quad (1)$$

Where, $k_1$ and $k_2$ is the kinetic constants of Fenton-like and photocatalytic process, respectively. $k_{12}$ is the kinetic constant of the combined photocatalytic Fenton-like process. The kinetic constants were calculated by fitting the experimental data with Langmuir-Hinshelwood model. The *pseudo* first order reaction equation was assumed because the concentration of BPA is very low. The correlation coefficients ($R^2$) for all the process are above 0.95, suggesting that the assumption is reasonable (Fig. 3B). The $S$

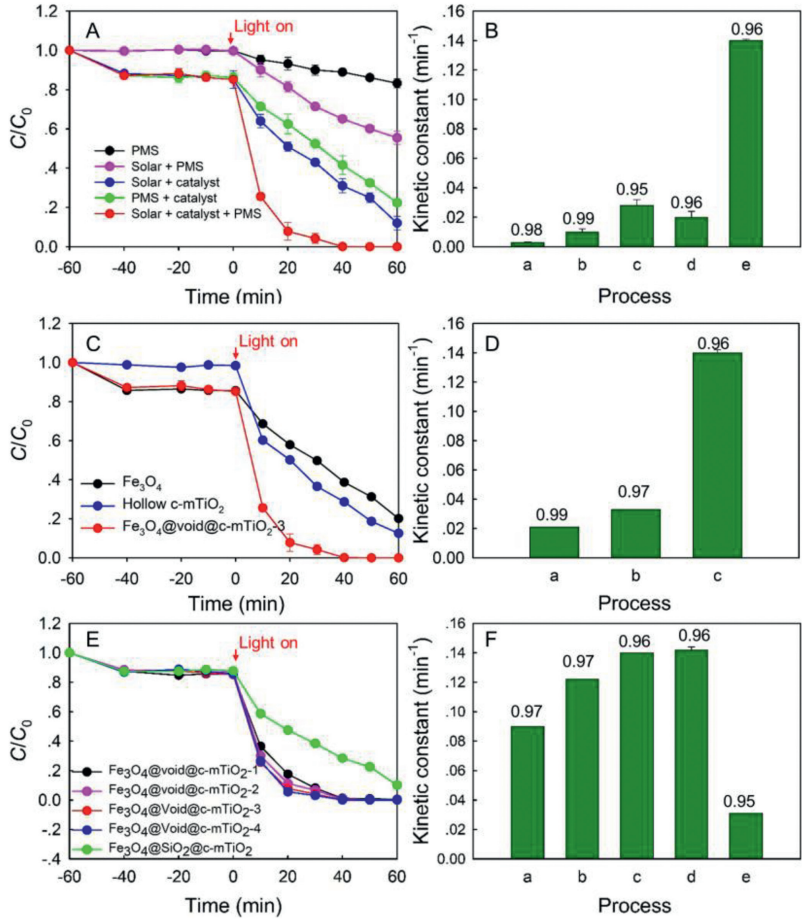


**Fig. 3.** Photocatalytic Fenton degradation performance for BPA with different processes (A) and corresponding kinetic constant value (B); in B, PMS (a), Solar + PMS (b), Solar + catalyst (c), PMS + catalyst (d), and Solar + catalyst + PMS (e). Photocatalytic Fenton degradation performance for BPA (C) and corresponding kinetic constant value (D) in the presence of different catalysts; in D, $Fe_3O_4$ (a), Hollow c-m$TiO_2$-2 (b), and $Fe_3O_4$@void@c-m$TiO_2$-3 (c), $Fe_3O_4$@void@c-m$TiO_2$-4 (d) and $Fe_3O_4$@$SiO_2$@c-m$TiO_2$ (e). Photocatalytic Fenton degradation performance for BPA (E) and corresponding kinetic constant value (F) in the presence of catalysts with different void space; in F, $Fe_3O_4$@void@c-m$TiO_2$-1 (a), $Fe_3O_4$@void@c-m$TiO_2$-2 (b), $Fe_3O_4$@void@c-m$TiO_2$-3 (c), $Fe_3O_4$@void@c-m$TiO_2$-4 (d) and $Fe_3O_4$@$SiO_2$@c-m$TiO_2$ (e).

is calculated to be 2.9, much larger than 1, suggesting that the combined process is not a simple sum of photocatalytic and Fenton-like process. The total leached iron ions concentration after the reaction was also measured at the neutral condition (Fig. S4 in Supporting information). We found that when only the catalyst was added to the system, negligible iron ions was detected, suggesting that the catalyst is stable. After the irradiation of solar light, the concentration of leached Fe ions increased, which is possibly due to that the structural $Fe^{3+}$ ions on the surface of $Fe_3O_4$ lose their stability after scavenging the photo-excited electrons and thus get detached from the surface and then leached into the solution (Fig. S4b). The combination of PMS with the catalyst could also lead to the generation of a small amount of leached Fe ions, resulted from the mutual activation of PMS and catalyst surface. When combining these three together, the concentration of more than 20 times larger for leached Fe ions was detected, suggesting a strong synergistic interaction between these elements. This agrees well with the performance results. To demonstrate the superiority of the micro-reactor system, the degradation performances of individual $Fe_3O_4$ and hollow structured mesoporous c-$mTiO_2$ ($Fe_3O_4$ was etched out by a hot HCl solution) under solar light in the presence of PMS were also examined. It is clearly shown that both the photocatalytic Fenton-like degradation performances of $Fe_3O_4$ and hollow structured mesoporous c-$mTiO_2$ are much smaller than that of the $Fe_3O_4$@void@c-$mTiO_2$-3 micro-reactor, indicating that necessity to construct such a catalyst (Fig. 3C). In addition, the photocatatyic performance of hollow structured mesoporous c-$mTiO_2$ in the presence of PMS is larger than that without PMS, revealing that PMS also promote the photocaltyic reaction owing to the scavenge of photo-excited electrons (Fig. S5 in Supporting information). According to the calculated kinetic constant (Fig. 3D), the synergistic factor is derived to be 2.5, further revealing the great enhancement after combining $Fe_3O_4$ and hollow c-$mTiO_2$ together.

The effect of void size on the degradation performance was also evaluated (Figs. 3E and F). It is clear that the core-shell structured $Fe_3O_4$@$SiO_2$@c-$mTiO_2$ without etching out the $SiO_2$ interlayer shows a much smaller photocatalytic Fenton-like degradation performance than that the samples with void space, suggesting that the void space plays an important role in promoting the catalytic performance. This is because the presence of void space can not only increase the number of exposed reactive sites of inner core, thus facilitating the Fenton-like catalytic performance, but also promote the enrichment of the organic pollutants and PMS in the void space, bringing the synergistic effects between the photocatalytic and Fenton-like catalytic process. We also found that the photocatalytic Fenton-like degradation rate of BPA increased with the increase of void space size. This result is reasonable because larger void possess more space for the confined reaction between the photocatalytic and Fenton-like reaction. However, further increasing the void space beyond 70 nm did not lead to a significant increase in the degradation reaction rate, possibly owing to that too large void space will also reduce the synergistic interaction between the two reactions. Therefore, the $Fe_3O_4$@void@c-$mTiO_2$-3 was used for the subsequent test.

The pH is an important factor to be considered for the practical application of Fenton based process. Thus, the degradation performance of $Fe_3O_4$@void@c-$mTiO_2$-3 was also investigated at different pH (Fig. 4A). We found that in this system, the removal efficiency in both acidic and neutral condition is similar, indicating that this catalyst can work in a neutral pH, which is favorable for the practical application. However, the removal efficiency sharply decreased when the pH was adjusted to 10 possibly owing to the change of reaction mechanism. It is speculated that on the $Fe_3O_4$ nanoparticles, the mechanism could be proposed as follows (Eqs. 2–4) [25–27]. Where, the $\equiv$ symbol indicates the species on the surface of $Fe_3O_4$ nanoparticles.

$$\equiv Fe(II) + HSO_5^- \rightarrow \equiv Fe(III) + SO_4^{2-} + {}^{\bullet}OH \quad (2)$$

$$\equiv Fe(II)^- OH + HSO_5^- \rightarrow \equiv Fe(II)(HO)OSO_3^- + OH^- \quad (3)$$

$$\equiv Fe(II)(HO)OSO_3^- \rightarrow Fe(III)^- HO + SO_4^{\bullet -} \quad (4)$$

According to these equations, the reaction mechanism could be different at acidic and basic condition. At an acidic/neutral condition, the ferric ions could directly react with PMS to generate

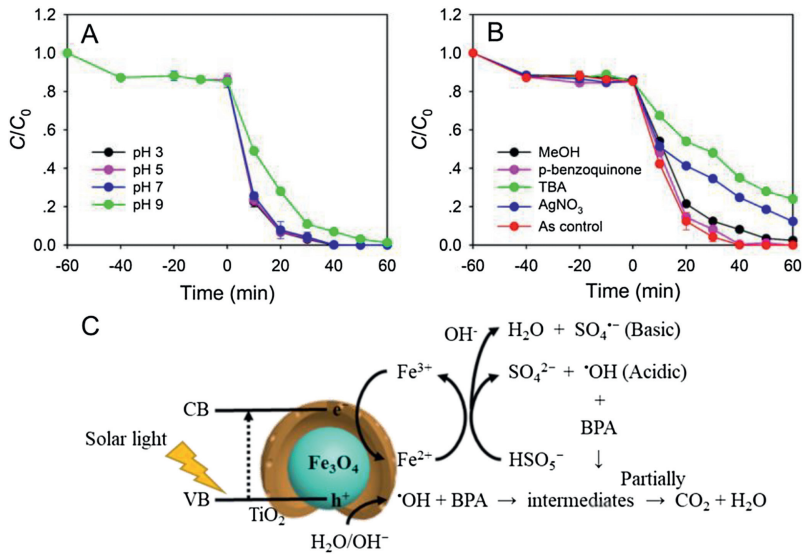


**Fig. 4.** Photocatalytic Fenton degradation performance for BPA with at different pH (A) and in the presence of different scavengers (B). Schematically illustrate the mechanism for photocatalytic Fenton degradation of BPA in the presence of yolk-shell structured mesoporous $TiO_2$ as the micro-reactor (C).

$^{\bullet}OH$ (Eq. 2). While in a basic condition, the system is abundant with negatively charged OH groups, which could be adsorbed on ≡Fe (II) ions to form ≡Fe(II)—OH complex. After addition of PMS, ≡Fe(II)—OH on the catalysts could first react with $HSO_5^-$ to generate ≡Fe(II)$(HO)OSO_3^-$ (Eq. 3) that subsequently decomposed to $SO_4^{\bullet-}$ (Eq. 4). Consequently, Fe(II) would transform to Fe(III). Owing to the lower oxidation potential of $SO_4^{\bullet-}$ than $^{\bullet}OH$, thus the performance of this catalyst in basic condition is less effective than that in acidic condition. The recycling test of the $Fe_3O_4$@void@c-$mTiO_2$-3 micro-reactor at pH 7 was also tested (Fig. S6 in Supporting information). After five recycles, no apparent decrease in the degradation kinetic constant was observed, indicating the excellent reusability of the catalyst. Both the SEM and TEM images of the recycled samples have shown that the well-defined core-shell structure were well retained, suggesting the excellent stability of the micro-reactor. However, the particle size of the inner magnetite cores slightly decreased, which is due to the iron leaching during the reaction. There is no clear change in the XRD pattern, revealing that the crystal structure of the catalyst was well maintained (Fig. S7 in Supporting information). To further clarify the reactive species involved in the reaction system, the scavenging tests were carried out in neutral condition (Fig. 4B). The addition of a scavenger for $^{\bullet}OH$ (*tert-butyl* alcohol) dramatically suppressed the combined photocatalytic Fenton-like reaction, suggesting that the $^{\bullet}OH$ was the dominate species [28]. A slight decrease of the degradation performance in the presence of p-benzoquinone (BQ) for $^{\bullet}O_2^-$, indicating that $^{\bullet}O_2^-$ degradation was not significant [18]. Besides, the introduction of $AgNO_3$, as a scavenger for photo generated electrons ($e^-$), had a strong effect on the performance for degrading BPA, suggesting that $e^-$ was also the dominate species. This is possibly because the addition of $AgNO_3$ scavenged the photo-generated electrons, thus inhibiting the recombination of photo-generated charges [29]. This result is different from that occurs in photocatalytic process, holding the fact that if the $Ag^+$ consumed the electrons, more holes would survive and thus could generate more $^{\bullet}OH$. However, in this combined system, the Fenton-like reaction was also involved, which constructs the relationship with the photocatalytic process by scavenging the electrons with the $Fe^{3+}$. The $Ag^+$ would capture most electrons because it has a higher oxidation potential than $Fe^{3+}$ and thus the interactions between the Fenton-like and photocatalytic process could be inhibited. While from the synergistic factor calculation, we can see that the performance enhancement from the synergy is much larger than that by the individual process. As a final result, the overall reaction rates are reduced upon the addition of $Ag^+$. In the PMS involved Fenton reaction, the generation of $SO_4^{\bullet-}$ usually occurs. Therefore, the methanol (MeOH) was added to examine the effect of $SO_4^{\bullet-}$. However, very little decrease in the degradation performance was found suggesting that $SO_4^{\bullet-}$ is not the directly reactive species responsible for BPA degradation [10,30].

Based on the results above, the mechanism can be explained by Fig. 4C that BPA molecules are mainly degraded by $^{\bullet}OH$, which are produced by several pathways. The irradiation of solar light could excite the outer $TiO_2$ shell to generate photo-excited electrons and holes at the conduction band (CB) and valance band (VB), respectively. Then, the holes can react with the water molecules or $OH^-$ to generate $^{\bullet}OH$. At the same time, the ferric ion can activate the PMS to generate sulfate radicals and ferrous ions. At this moment, the ferrous ions plays an important role in keeping the interaction between the $TiO_2$ shell based photocatalytic and $Fe_3O_4$ based Fenton process because on one hand, the $Fe^{3+}$ can scavenge the photo-excited electrons, thus greatly inhibiting the recombination of electrons and holes. Note that the PMS could also scavenge the photo-excited electrons, but from the experiment result (Fig. S5), the scavenge effect is not significant; on the other hand, the $Fe^{3+}$ can be recovered quickly to generate $Fe^{2+}$ to promote the Fenton-like reaction. It is well known that the lifetime of these radicals is very short, which can be easily recombined to form $H_2O_2$ or $SO_4^{2-}$, exhibiting a much smaller oxidation potential. The presence of void spaces can effectively reduce this effect because they can provide enough space to enrich the BPA modules to get close to the radicals, thus achieving an excellent degradation performance. Finally, the radicals can oxide the BPA molecules to small intermediates and then partially be mineralized into $CO_2$ and $H_2O$, which has been proved by the total organic carbon (TOC) degradation test.

In summary, we have successfully prepared the yolk-shell structured $Fe_3O_4$@void@c-$mTiO_2$ micro-reactor through a combined Stöber coating method and an ultrasound assisted etching process. The $Fe_3O_4$@void@c-$mTiO_2$ NPs with a high specific surface area and a well-defined yolk-shell structure exhibit a remarkable performance for degrading BPA due to the synergic effect between the $TiO_2$ shells based photocatalytic process and the $Fe_3O_4$ cores based Fenton-like reaction. More importantly, the void space can act as a micro-reactor, providing a special place for the catalytic reaction. Furthermore, the catalyst can work efficiently in both acidic and neutral condition. Owing to the high magnetization, the catalyst can be conveniently recovered by a hand-held magnet and be recycled for 5 times without significant loss of activity. This study provides a novel way for the design of unique micro-reactor catalyst for the photocatalytic Fenton-like reaction.

## Declaration of competing interest

The authors declare that they have no known competing financial interests or personal relationships that could have appeared to influence the work reported in this paper.

## Acknowledgments

This work is supported by the National Natural Science Foundation of China (Nos. 51822202219721 63 and 51772050), the Fundamental Research Funds for the Central Universities (No. 2232020D-02), Shanghai Sailing Program (No. 20YF1400500), Shanghai Natural Science Foundation (No. 20ZR1401500), Shanghai Rising-Star Program (No. 18QA1400100), Youth Top-notch Talent Support Program of Shanghai, Science and Technology Commission of Shanghai Municipality (No. 19520713200), Shanghai Scientific and Technological Innovation Project (No. 19JC1410400), Key Basic Research Program of Science and Technology Commission of Shanghai Municipality (No. 20JC1415300), DHU Distinguished Young Professor Program and Fundamental Research Funds for the Central Universities.

## Appendix A. Supplementary data

Supplementary material related to this article can be found, in the online version, at doi:https://doi.org/10.1016/j.cclet.2020.09.061.

## References

[1] A. Pal, K.Y.H. Gin, A.Y.C. Lin, M. Reinhard, Sci. Total Environ. 408 (2010) 6062–6069.
[2] D.J. Lapworth, N. Baran, M.E. Stuart, R.S. Ward, Environ. Pollut. 163 (2012) 287–303.
[3] R. Loos, R. Carvalho, D.C. António, et al., Water Res. 47 (2013) 6475–6487.
[4] I. Bautista-Toledo, M.A. Ferro-García, J. Rivera-Utrilla, C. Moreno-Castilla, F.J. Vegas Fernández, Environ. Sci. Technol. 39 (2005) 6246–6250.
[5] D.P. Mohapatra, S.K. Brar, R.D. Tyagi, R.Y. Surampalli, Chemosphere 78 (2010) 923–941.
[6] I. Gültekin, N.H. Ince, J. Environ. Manage. 85 (2007) 816–832.
[7] M. Cheng, G. Zeng, D. Huang, et al., Chem. Eng. J. 284 (2016) 582–598.

[8] N.N. Mahamuni, Y.G. Adewuyi, Ultrason. Sonochem. 17 (2010) 990–1003.
[9] Y. Yang, J.J. Pignatello, J. Ma, W.A. Mitch, Environ. Sci. Technol. 48 (2014) 2344–2351.
[10] H. Lu, M. Sui, B. Yuan, J. Wang, Y. Lv, Chem. Eng. J. 357 (2019) 140–149.
[11] C. Zhu, F. Liu, C. Ling, et al., Appl. Catal. B: Environ. 242 (2018) 238–248.
[12] L. Dong, T. Xu, W. Chen, W. Lu, Chem. Eng. J. 357 (2019) 198–208.
[13] E. Neyens, J. Baeyens, J. Hazard. Mater. 98 (2003) 33–50.
[14] S. Caudo, G. Centi, C. Genovese, S. Perathoner, Top. Catal. 40 (2006) 207–219.
[15] P. Qiu, K. Kang, K. Kim, et al., RSC Adv. 5 (2015) 96201–96204.
[16] S.Q. Liu, L.R. Feng, N. Xu, Z.G. Chen, X.M. Wang, Chem. Eng. J. 203 (2012) 432–439.
[17] Y. Ling, M. Long, P. Hu, Y. Chen, J. Huang, J. Hazard. Mater. 264 (2014) 195–202.
[18] H. Yi, M. Jiang, D. Huang, et al., J. Taiwan Inst. Chem. Eng. 93 (2018) 184–192.
[19] L. Xu, J. Wang, Environ. Sci. Technol. 46 (2012) 10145–10153.
[20] X. Qian, M. Ren, Y. Zhu, et al., Environ. Sci. Technol. 51 (2017) 3993–4000.
[21] R.R. Solís, F.J. Rivas, A.M. Chávez, D.D. Dionysiou, J. Hazard. Mater. 400 (2020) 123118.
[22] Y. Xu, J. Ai, H. Zhang, J. Hazard. Mater. 309 (2016) 87–96.
[23] S. Luo, L. Duan, B. Sun, et al., Appl. Catal. B: Environ. 164 (2015) 92–99.
[24] H. Sun, C. Kwan, A. Suvorova, et al., Appl. Catal. B: Environ. 154–155 (2014) 134–141.
[25] Z. Wu, Y. Wang, Z. Xiong, et al., Appl. Catal. B: Environ. 277 (2020)119136.
[26] W. Oha, Z. Dong, T. Lima, Appl. Catal. B: Environ. 194 (2016) 169–201p.
[27] C. Tan, N. Gao, Y. Deng, et al., J. Hazard. Mater. 276 (2014) 452–460.
[28] T. Zeng, X. Zhang, S. Wang, et al., Chem. Eur. J. 20 (2014) 6474–6481.
[29] D. Du, W. Shi, L. Wang, J. Zhang, Appl. Catal. B: Environ. 200 (2017) 484–492.
[30] J. Wang, S. Wang, Chem. Eur. J. 334 (2018) 1502–1517.